Liquid-liquid phase separation in borosilicate glass enriched in MoO3 – experimental investigations and thermodynamic calculations

Sophie Schuller, Pierre Benigni, Stéphane Gossé, Sébastien Bégaud-Bordier, Georges Mikaelian, Renaud Podor, Jacques Rogez

Liquid-liquid phase separation in borosilicate glass enriched in MoO_3 – experimental investigations and thermodynamic calculations

Sophie Schuller[1*], Pierre Benigni[2], Stéphane Gossé[3], Sébastien Bégaud-Bordier[4], Georges Mikaelian[2], Renaud Podor[1] Jacques Rogez[2]

[1]CEA, DES, ISEC, Université Montpellier, Marcoule, France

[2]Aix Marseille Univ, Université de Toulon, CNRS, IM2NP, Marseille, France

[3]DES, ISAS – Service de la Corrosion et du Comportement des Matériaux dans leur Environnement (SCCME), CEA, Université Paris-Saclay, F-91191, Gif-sur-Yvette, France

[4]Orano DS F-91191 Gif-sur-Yvette

*Corresponding author: sophie.schuller@cea.fr

Abstract

Phase separation in sodium borosilicate glasses containing molybdenum oxide has been studied in a compositional range of interest for nuclear glasses. Two series of quaternary compositions $(63.5SiO_2\text{-}19.6Na_2O\text{-}16.9B_2O_3)_{1-x}(MoO_3)_x$ with $0 \leq x \leq 3$ mol.% MoO_3 have been synthesized and characterized, by a range of complementary experimental techniques both in situ in temperature, by viscometry and hot stage SEM, and ex-situ, by HRTEM, PXRD, EPMA and dissolution calorimetry. The phase separation temperatures between silicate and molybdenum oxide rich liquids were determined for each composition. Molybdenum oxide solubility limits were established for quenched and annealed glasses.For molybdenum oxide contents exceeding these limits, crystalline sodium mono-molybdates precipitate in the glasses as shown by XRD results and the fractions of precipitates were indirectly quantified by MoO_3 mole balance and enthalpy balance relying on solution calorimetry experiments. The experimental results were compared with thermodynamic calculations performed with Thermo-Calc software and a CALPHAD database of the $SiO_2\text{-}Na_2O\text{-}MoO_3$ ternary system. The ternary model allows the calculation of the nature and quantity of the precipitated phases in reasonable agreement with the experiments, even if, in the current state of development of the thermodynamic database, the absence of boron restricts the relevance of the calculations. Thus, for the construction of a predictive thermodynamic calculation tool, the addition of boron to the database is the most promising prospect.

1 Introduction

In multi-component oxide glasses, complex phase separation phenomena may occur between stable or metastable liquid phases by spinodal decomposition (1) (2) or by nucleation and growth (3, 4). The spinodal decomposition mechanism, which leads to a microstructure formed by an intimate interweaving of the 2 phases, is used industrially for the manufacture of glasses with high thermal resistance, such as Vycor® and Pyrex®, and of porous glasses (5, 6). Phase separation by nucleation and growth leads to the appearance, within the glass matrix, of a dispersion of secondary phase precipitates, spherical in shape and disconnected from each other. This mechanism is observed in some radioactive waste glasses containing molybdenum oxide. Molybdenum, which is present in significant quantities in Uranium-Molybdenum spent fuel, in waste coming from the reprocessing of Uranium-OXide fuel and in waste coming from dismantling, has generally a low solubility, of the order of a few mol.% MoO_3, in borosilicate glasses.

Whereas, in R7T7 glasses, the molybdenum content remains below the solubility limit, in the above examples of industrial UMo glass (7-9), glass ceramics for the TRUEXplus waste stream (10-12) and glass for dismantling waste (13), the solubility limit is exceeded, liquid-liquid phase separation occurs and secondary phases are precipitated during cooling. Contrary to the case of glass-ceramics in which the as-cast glass is homogeneous and the microstructure is optimized by controlling the precipitation of the secondary phases by an adapted heat treatment (14, 15), the glass will be here heterogeneous at the microscopic scale from the as-cast state.

However, it is still possible to optimize the heterogeneous microstructure of nuclear glass by adjusting the composition of the glass matrix. For example, in a sodium-calcium borosilicate matrix, increasing the calcium content will promote the trapping of molybdenum in the form of calcium molybdate and enhance chemical resistance to water alteration (8, 16, 17). Calcium molybdate phase is less detrimental than sodium molybdate, whose lower melting point allows it to aggregate in liquid form, leading in the end to the presence of macroscopic secondary phases (18).

To carry out this fine optimization of nuclear glass compositions, it is therefore essential, firstly, to understand the thermodynamics of the processes involved, based on the structural knowledge of the glasses studied, and secondly, to progress in the construction and validation of a suitable thermodynamic calculation tool.

Structural studies of borosilicate glasses containing molybdenum oxide provide a first explanation for its low solubility. More specifically, it was shown that the Mo^{6+} species was the most thermodynamically stable when the glasses were synthesized under the air oxygen

partial pressure. EXAFS studies carried out by at the K threshold of Mo further showed that the Mo^{6+} ion is four-fold coordinated under the form of molybdate units (MoO_4^{2-}) and does not share any bridging oxygen with other network former cations (Si^{4+}, B^{3+}, Al^{3+}). The length of the Mo^{6+}-O^{2-} bond, of the order of 1.8 Å, varies little with the chemical composition of the silicate and borosilicate glasses and with the nature of the alkali and alkaline-earth metals present in the glasses studied (19) (20, 21) (8). These observations are completely consistent with the studies carried out by solid state MAS NMR of the ^{23}Na, ^{11}B, ^{28}Si, ^{95}Mo isotopes and by Raman spectroscopy which show, on the one hand, the presence of depolymerized zones of the glassy network, enriched in MoO_3, alkaline and alkaline-earth elements and, on the other hand, the presence of polymerized zones enriched in network former elements and depleted in MoO_3 (22-27). Although not fully proven by experiments probing the glass medium range order, these atomic scale structural arrangements are most likely the beginnings of phase separation between molybdate units and silicates.

After cooling and whatever the quenching rate, scanning and transmission electron microscopy observations of the microstructure of alkali or alkaline earth borosilicate glasses containing high levels of molybdenum oxide show that the MoO_3-enriched zones systematically have the appearance of spherical precipitates, dispersed in the matrix and disconnected from each other (9, 23, 28-31). It was also shown that these MoO_3 enriched zones were composed of a mixture of molybdate crystals of different natures such as, depending on the chemical composition of the initial glass, Na_2MoO_4 (24), $CsNaMoO_4$ (29) or $CaMoO_4$ (10, 23, 32), and a residual glass phase (15).

In the studies quoted above, the concept of MoO_3 solubility limit does not have a precise thermodynamic meaning, it simply represents the content of incorporation beyond which, after cooling, the observed glasses are no longer homogeneous, without specifying the temperatures at which the phenomena of phase separation occur, which are the phases involved, nor at what spatial scale(s) these phases are observed. On the contrary, in our study, we propose to clarify from an experimental and theoretical point of view the thermodynamics of phase separation in a simplified glassy system of nuclear interest containing MoO_3.

To this end, a series of quaternary SiO_2-Na_2O-B_2O_3-MoO_3 model glasses with varying molybdenum oxide content are synthesized and studied using a wide range of complementary experimental techniques. Quaternary compositions are obtained by adding a controlled amount of MoO_3 between 0 and 3 mol.%, to a reference ternary glass of composition $63.5SiO_2$-$19.6Na_2O$-$16.9B_2O_3$ (mol.%). Two distinct thermal paths are compared: the so called "quenched glasses" are cooled rapidly from 1300°C at an estimated rate of 10^3°C·min^{-1}, the so called "annealed glasses" were maintained 10 h at 650°C. A first series of investigations

was carried out on the glasses after cooling. The glass compositions were checked by EPMA. The morphology and the nature of the formed phases were determined by optical microscopy and TEM. Measurements by acid solution calorimetry at room temperature (33) allowed to determine the solubility limit in MoO_3 and to quantify the fractions of molybdate phases precipitated in the glasses.

The glasses were then analyzed according to temperature in order to specify the liquid demixing temperature for each MoO_3 content. Thus, the evolution of their microstructure during heating from room temperature to 900°C at constant rate (30 °C/min) was observed by hot stage scanning electron microscopy. Viscosity values were measured in isothermal mode at temperatures between 900 and 1350°C.

The acquired experimental data are finally compared to previous experimental results obtained on industrial borosilicate glass compositions of UMo type (9) and to the results of thermodynamic calculations performed with the Thermo-Calc software based on an available CALPHAD description of the SiO_2-Na_2O-MoO_3 ternary system (34).

2 Methodology

2.1. Preparation method and compositions of glass samples

The glasses are synthesized from a mixture of oxide (SiO_2, MoO_3,), borate (H_3BO_3) and carbonate (Na_2CO_3) precursor powders. After homogenization, a 100 g charge of mixture contained in a platinum-rhodium crucible is heated to 1300°C for 3 hours in a muffle furnace. The liquid obtained is then quenched by casting on a cooled copper hearth immediately followed by a crushing on this hearth with a second copper plate. The cooling rate reached is estimated to be 10^3°C·min^{-1}.

The optically homogeneous glasses are subsequently annealed. During this heat treatment, a mass of 100 mg of glass is taken, coarsely ground and loaded in an Au-Pt cup. The cup is placed in a tubular furnace at room temperature and heated at a rate of 1.5°C min^{-1} to 650°C, held at this temperature for 10 h and then air cooled.

2.2. PXRD (Power X-Ray Diffraction)

The analyzed samples are finely ground in order to avoid any preferential orientation of the grains. The diffractometer used is a Philips X'Pert Pro model in θ-θ geometry, equipped with a copper anticathode of wavelength 1.54 Å. Powder diffraction patterns are acquired in the 10-80° 2θ range with an angle step of 0.017° and time step of 2 s. The identification of the crystalline phases is carried out with the help of the EVA® software and by comparison of the

diffractograms with the crystallographic databases of the International Center of Diffraction Data (JCPDS files).

2.3. HRTEM

The HRTEM analyses were performed with a JEOL JEM 2010F UPR22 microscope (CP2M Aix-Marseille University, France) on the samples Na-Mo0 and Na-Mo1,5. The beam diameter is in the nanometer range under an accelerating voltage of 200 kV. The samples are crushed and dispersed in absolute alcohol. They are then deposited on a copper grid. This equipment allows high resolution analyses to be performed (HRTEM).

2.4. EPMA

The chemical compositions of the glasses were measured with a CAMECA SX100 electronic microprobe, using crystals LPET for the measurement of molybdenum, LPC3 for boron, and LTAP for sodium and silicon. The electronic beam operating voltage and current were 12 kV and 10 nA respectively. The analysis conditions were optimized to minimize sodium migration under the beam. The acquisition time was set at 70 seconds and the defocused beam size at 45 micrometers for all analyses. 10 analysis points per sample were performed.

2.5. Solution calorimetry

Solution calorimetry consists in measuring the enthalpy associated with the dissolution reaction of a solute sample in a liquid solvent at controlled temperature. This enthalpy evolves with the chemical composition of the solute and the concentration of the solute in the solvent. The thermodynamic functions of a solution, a phase with variable composition, necessarily evolve with the chemical composition of the solution (33).

Experimentally, the study by dissolution calorimetry of a binary A-B, ternary A-B-C or multicomponent solution, whose extension in composition is sometimes not well known, is most often carried out by dissolving a series of samples with increasing content of one of the constituents of the solution, for example A.

If all the samples in the series are single-phase, the curve of evolution of the measured enthalpy vs. A content does not present any remarkable accident, the slope of the curve remains continuous in the explored composition interval as shown in figure 1 by the experimental enthalpy curve at 1450 K (scatter symbols).. On the other hand, if a fraction of the samples of the series are, for example, biphasic, the recorded thermograms correspond to the weighed sum of two, one for each phase, independent dissolution effects. As, in the general case, the enthalpy of dissolution of the second phase differs from that of the studied solution, it is observed a slope break on the enthalpy curve vs. A content. This slope break is a thermal

signature of the crossing of a solubility limit, associated with the presence of a non-zero fraction of the second phase.

If the solution is a binary mixture A-B, the enthalpy will evolve linearly with the content of A (or B), within the series of two-phase samples, as shown in figure 1 by the linear segment of the calculated enthalpy curve at 1380 K (black solid line). If the solution is a ternary mixture A-B-C, the situation is more complex. The compositional trajectory followed with increasing A content is in general not aligned with the conodes in the two-phase domain. The evolution of the enthalpy is then no longer constrained to evolve linearly with the A content. However, as in the binary case, a slope break can still be observed when the solubility limit is crossed.

This method is used here to characterize the precipitation of molybdates in the Na-Mo*x* glass series.

Hydrofluoric acid being the only acid that attacks siliceous compounds at room temperature, its presence in the solvent is unavoidable. The ground samples are therefore dissolved at 25°C in 8 ml of an aqueous acid solution HF-6M, HNO_3-4M in a high sensitivity (15.6 µW/µV) tilting calorimeter calibrated in energy by the dissolution reaction of THAM in an aqueous solution of 0.1 M HCl (35).

In aqueous solvents, the enthalpy of dissolution can vary greatly with solute concentration and enthalpy of mixing at infinite dilution is obtained by extrapolation of measurements at varying concentrations. However, by carrying out the dissolutions at a fixed and low concentration, the curve obtained can be assimilated, without much error, to the curve at infinite dilution. In our experiments, the solute concentrations were between 10.2 and 11.8 mmol (of oxides).L^{-1} (of solvent).

In the samples, the major phase, which is the borosilicate glassy matrix, dissolves easily in the acid mixture and the recorded thermograms always show a correct return to the initial baseline. Moreover, even in the case of biphasic samples, no cloudy solution, which would be indicative of insoluble phases, was ever observed after dissolution. Thus, it appears that all the samples studied are completely dissolved under the experimental conditions of our calorimetric experiments. The secondary phase crystallized in small quantities was identified as mono-molybdate Na_2MoO_4. As an additional precaution, dissolution tests of this pure compound in the same solvent allowed to verify its complete dissolution.

At high and constant dilution, the measured thermal effects are not disturbed by possible interactions between solute elements in the solvent. From one sample to another, the concentrations reached in the solvent after dissolution, as for example the concentrations of

MoO_4^{-2} molybdate ions, are very close and thus the final states and the measured energies are representative of the initial states of the samples.

2.6. Viscometry

Since the early 1970s (36) (37, 38), (39) viscosity measurement has been used to demonstrate the onset of liquid-liquid phase separation in sodium borosilicate glasses. More recently (9), and for the same purpose, the technique was applied to the case of sodium borosilicate glasses containing phosphorus and high amounts of molybdenum oxide (> 6 mol.%). The same methodology is used again for the series of Na-Mo*x* glasses studied in this work.

The rheological behavior of the liquid is measured at high temperature with a co-axial cylindrical rotating viscometer of the Searle type. The viscometer consists of two coaxial cylinders. The platinum-rhodium crucible of 27 mm inner diameter is fixed. The platinum-rhodium rotor of diameter 9 mm, is coupled to a Rheometric Scientific rheometer which ensures the control of the rotation speed and measures the torque resulting from the immersion of the rotor in the molten glass.

A glass volume of 21 cm^3 is needed for the viscosity measurement. The filling of the crucible requires several successive operations of addition/melting of glass, operations carried out in an auxiliary furnace beforehand heated to the glass synthesis temperature. The measurement protocol is as follows. After filling and cooling, the crucible is placed in the viscometer and heated at 5°C/min until the target temperature is reached. This temperature is measured by a type S thermocouple in contact with the crucible.

For each temperature, after a thermal stabilization of 30 to 45 min, the rheological behavior of the liquid is analyzed at increasing rotor speed from 0 to 100 rpm and then decreasing from 100 to 0 rpm. The duration of this isothermal analysis is 5 min with a total of 240 measurement points acquired. The viscosity of the liquid is determined by linear regression between shear stress and strain rate. If the liquid is homogeneous, the viscosity curves measured at increasing and decreasing rotor speed are superimposed, indicating a Newtonian behavior. On the other hand, as soon as the liquid undergoes a phase separation, two distinct curves are recorded during the measurements at increasing and then decreasing rotation speed because the viscosity continuously drifts with time during the measurements. This characteristic evolution indicates a transition from a Newtonian to a non-Newtonian behavior.

The range of measurable viscosities is between 0.5 Pa.s and 240 Pa.s corresponding, in the case of sodium borosilicate glasses, to the temperature range 900-1500°C. The isothermal measurements are first performed at decreasing temperatures and then, at the end of the experiment, the glass is heated up to a temperature between 1250°C and 1350°C to evaluate

the reversibility of its rheological behavior after a stay below the phase separation temperature. The overall uncertainty of the viscosity measurement is < 10%.

When the MoO_3 content of the glasses is less than or equal to 1 mol.%, the phase separation temperature becomes lower than 900°C, the viscosity higher than 3000 dPa s^{-1} of the mixture at this temperature is then likely to block the viscometer rotor. It is necessary to use an alternative experimental technique to determine the phase separation temperature. The ESEM technique was then adopted for in situ analysis of the glasses during heating.

2.7. *In situ* electron microscopy

The microscope used is a FEI QUANTA 200 ESEM FEG equipped with a heating stage (25-1500°C) (40), (41) and a measurement thermocouple of S type. The difference between the set and measured temperatures is estimated at 25°C between 600 and 800°C. The quenched glass to be studied is placed in an Au-Pt crucible of 5 mm diameter, itself placed on the heating stage of the microscope. The crucible is then heated at a constant 30°C/min rate from room temperature to 850°C under an air pressure of 250 Pa. The electron beam is accelerated under a voltage of 30 kV. Images are acquired every 5 seconds.

Preliminary tests of *in situ* observation of the evolution of the microstructure of the glasses on heating were carried out. For glasses containing a MoO_3 content < 1 mol.%, no phase separation could be detected. For glasses with a MoO_3 content > 1 mol.%, a crystallization of silicate phases on the surface of the sample occurs under the electron beam. These precipitations are an artefact linked to the observation technique, the observed phases are not representative of the behavior of the glass under classical heating conditions. It is therefore not possible to obtain a reliable estimate of the phase separation temperature for these glasses. Thus, relevant results could only be obtained for the Na-Mo1 glass containing 1 mol.% MoO_3.

2.8. CALPHAD calculations

In order to gain a better insight into the observed demixing phenomena, thermodynamic calculations have been performed with the CALPHAD methodology (42) using the Thermo-Calc software (43). The calculations are based on the MoO_3-Na_2O-SiO_2 ternary database developed by S. Bordier during his PhD thesis (44). In this database, the description of the Na_2O-SiO_2 binary is taken from (45) while the modelling of the two other binary subsystems, MoO_3-SiO_2 and Na_2O-MoO_3, is an original assessment from the thesis. The two MoO_3-Na_2O-SiO_2 isothermal sections determined experimentally by Stemprok (46) (47) were used for the optimization of the ternary system.

Although B_2O_3 is not included in this database, the phenomena of demixing and precipitation of molybdates can be calculated. Indeed, these phenomena have their origin in the repulsive interaction that exists within the liquid phase between MoO_3 and SiO_2. This binary repulsive interaction extends in the Na_2O-MoO_3-SiO_2 system and results in a large ternary miscibility gap.

The comparison of experimental results obtained on MoO_3-Na_2O-B_2O_3-SiO_2 quaternary glasses with calculations based on a purely ternary thermodynamic description, in which B_2O_3 is not taken into account, imposes to simplify the composition of the experimental glasses in the calculations. Considering that B_2O_3 and SiO_2 both play the role of network formers in the glass structure, we have chosen to represent the B_2O_3 content of the experimental glasses by adopting in the calculations a SiO_2 content (80.4 mol.%) equal to the sum of the SiO_2 (63.5 mol.%) and B_2O_3 (16.9 mol.%) contents of the experimental glasses.

The thermodynamic modeling allows in particular to calculate the extension of the liquid miscibility gap in the phase diagram, and as a function of the MoO_3 concentration, the liquid-liquid phase separation temperature as well as the nature and the fractions of the phases formed upon cooling under equilibrium conditions.

Early calculations of the solidification path showed that in addition to molybdate precipitation, secondary phases such as crystalline silica and sodium silicates could form from the liquid during cooling. However, these SiO_2-rich crystalline phases are never observed experimentally in rapidly quenched glasses. Furthermore, they do not exhibit any Mo solubility in their structures. In order to focus on the molybdate interactions and to compare the thermodynamic calculations with the experimental results, the SiO_2-rich solid phases were suspended during the calculations. The results obtained correspond to metastable equilibria between the molybdate phases of the Na_2O-MoO_3 system and a solidified ternary liquid.

3 Results

3.1. Structural and microstructural analyses

The quenched glasses are visually transparent up to a concentration of 1.8 mol.% MoO_3 (Fig. 2). Above this concentration, white opalescence can be observed. It should be noted that the blue and brown iridescences observed are optical artefacts due to glass surface alteration in the quenching process. The compositions of the glasses measured by EPMA are in good agreement with the theoretical compositions derived from the weightings (see table 1) up to a content of 2 mol.%. Above this concentration, glasses containing separated phases dispersed in the residual glassy matrix are difficult to analyze.

For the quenched glasses, HRTEM analysis shows that the Na-Mo0 glass is homogeneous at the nanometric scale. However, spherical precipitates (5 to 10 nanometers) dispersed in the glass matrix are observed in the glass containing 1.5 mol.% MoO_3. The inter-plane fringes highlighted on the magnified image of a precipitate (Fig. 3) testify to their crystalline character. The XRD results (Fig. 4-a) show that crystals of di-hydrated sodium molybdate Na_2MoO_4-$2H_2O$ of orthorhombic structure and sodium mono-molybdates Na_2MoO_4 of δ-hexagonal and γ-orthorhombic structures are detected in the glasses containing 1.8 mol.% MoO_3. The intensities of the diffraction peaks, weak in the Na-Mo1.8 glass, increase significantly with the amount of molybdenum oxide contained in the glasses. These results attest to the presence of separate phases partially crystallized as sodium molybdates in samples containing 1.5 mol.% or more of MoO_3. The absence of diffraction peaks in the Na-Mo1.5 glass, for which crystalline precipitates were detected by TEM, is probably explained by a fraction of crystals too small to be detected by XRD.

The presence of γ-orthorhombic and δ-hexagonal crystals can be explained by the high cooling rate involved in the quenching operation after synthesis at 1300°C, allowing these high temperature forms to be observed at room temperature in a metastable state. The stable structure of sodium mono-molybdate at room temperature is the α-cubic form which was not detected in our experiments, instead a di-hydrate phase was observed. This surprising observation can be explained by considering that sodium molybdate, like other alkali mono-molybdates, is hygroscopic. It is therefore likely that the small amount of cubic phase initially present in our sample after quenching was completely converted to di-hydrate. It is also not excluded that a fraction of the detected di-hydrate also comes from the conversion of the γ and δ crystal amounts. Nicoleau et al. (24) were able to detect 18-36 wt.% of cubic crystals of sodium mono-molybdate in their quenched Na-Mo*x* samples with MoO_3 contents between 2 and 10 mol.%. The reason could be a shorter exposure of their samples to air humidity between the quenching operation and the PXRD analyses than in our experiments and/or the higher MoO_3 content of their samples, thus containing a larger amount of crystals and possibly a larger fraction of non-hydrated crystals.

The annealed glasses (Fig. 4-b) are visually homogeneous for MoO_3 contents lower than 0.8 mol.%. The presence of sodium molybdates of the same nature as in the case of quenched glasses is detected from 0.5 mol.% MoO_3. These glasses were annealed at 650°C, the temperature at which the δ-hexagonal structure is the stable form. Therefore, we would logically expect a larger δ-phase fraction to be present in the annealed samples. Since the Rietveld refinement was not performed, a quantitative assessment of the phase fractions is not available. However, it should be noted that the annealed samples were not quenched after

annealing, but simply removed from the furnace and allowed to cool in a still air atmosphere. During this not so rapid cooling stage, the high temperature δ-hexagonal form could be partially converted to the γ-orthorhombic form. The presence of the di-hydrate and the absence of the other allotropic forms can be explained by the same reasoning as for the quenched glasses.

3.2. Phase separation temperatures

Viscosity measurements on Na-Mo0, Na-Mo1.5, Na-Mo1.8, Na-Mo2.5 and Na-Mo3 systems as a function of shear rate ($\dot{\gamma}$) at different temperatures, are presented in Figure 5. For each system, are determined i) the maximum temperature T_{maxS} associated with the observation of a non-Newtonian behavior during viscosity measurements at increasing and then decreasing shear rate, ii) the minimum temperature T_{minS} (> T_{maxS}) at which the liquid remains Newtonian.

The temperature values T_{minS} and T_{maxS} are given in Table 2 for each glass. The average of the two temperatures is used to estimate the phase separation temperature and the associated standard deviation. The results show that the liquid is Newtonian over a decreasing temperature range as the molybdenum oxide concentration increases.

The *in situ* analysis of the Na-Mo1 glass by hot-stage ESEM on heating at 30°C/min from room temperature to 900°C allows us to observe the formation then the dissolution of separated phases in the glass matrix and to specify the characteristic temperatures associated with these phenomena. Between 652 and 702°C (Fig. 6), the separated phases initially present in the glass after cooling become liquid. This observation is consistent with the value of the melting temperature of Na_2MoO_4 (680°C) (48) major constituent of these phases. The quantity of separated phases subsequently increases between 702°C and 745°C then, the phases dissolve between 752 and 802°C, temperature for which the microstructure becomes completely homogeneous. We thus determine an average phase separation temperature of the Na-Mo1 glass equal to 777±25°C. The evolution of the phase separation temperature is plotted as a function of the MoO_3 content in Figure 12.

3.3. Solution calorimetry

In the glasses studied, as explained above (§ 2.5), the solubility limit of MoO_3 results in a slope break on the enthalpy curve measured as a function of MoO_3 concentration. Beyond the change of slope, the measured enthalpy follows a quasi-linear evolution despite the quaternary composition of the samples which are mixtures of four oxides. The solubility limit is measured at 1.5 mol.% MoO_3 in the case of quenched glasses (Fig. 7) and 0.5 % in annealed glasses (Fig. 8). The scattering of the measurements, which remains relatively low on the dissolution enthalpy curve of translucent and or opalescent glasses (Fig. 7 and 8), becomes relevant for samples with a molar MoO_3 content higher than 3% (results not presented here). This

increased dispersion results from the macroscopic phase separation produced when the glasses reach MoO_3 contents well above the solubility limit. It is explained by a sampling becoming heterogeneous which generates a greater dispersion in the dissolution enthalpy measurements. It should be noted that this is also the case for the measurements of viscosity in temperature.

For quenched and annealed glasses, it is possible to estimate the fractions of precipitated phases by a molybdenum oxide material balance (F_m fractions table 3). We consider that the glass samples containing a MoO_3 content higher than the solubility limit comprise a precipitated phase which is a mono-molybdate Na_2MoO_4 and a residual glass whose composition, close to that of the glass at the solubility limit, is not known. It will then be assumed that this composition has a MoO_3 content identical to that of the glass at the solubility limit. We will make the additional approximation that, for all the glass compositions studied in the two-phase domain, the composition of the residual glass is the same.

With the above assumptions, F_m then reads: $F_m = \frac{x_g - x_{rg}}{x_{moly} - x_{rg}}$

In the above equation, x_g, x_{rg} and x_{moly} are the MoO_3 mole fractions in the glass, the residual glass and the molybdate respectively. We hence have x_{rg} = 1.5 % and x_{rg} = 0.5 % for the quenched and annealed glasses respectively and x_{moly} = 50 %.

The precipitated phase fractions can alternatively be calculated by enthalpy balance (F_h fractions table 3). We write that the measured dissolution enthalpy is the sum of the dissolution enthalpies of the residual glass and the Na_2MoO_4 precipitates. The exact value of the dissolution enthalpy of the residual glass associated to each sample is not known, we will assume in first approximation that this glass remains unchanged and thus that its enthalpy of dissolution is the one of the glass whose composition corresponds to the measured solubility limit.

With the above assumptions, F_h then reads: $F_h = \frac{\Delta H_g - \Delta H_{rg}}{\Delta H_{moly} - \Delta H_{rg}}$
In the above equation, ΔH_g, ΔH_{rg} and ΔH_{moly} are the dissolution enthalpies of the glass, the residual glass and the molybdate respectively. We hence have ΔH_{rg} = $-142.09\ kJ\ mol\ oxides^{-1}$ and ΔH_{rg} = $-142.94\ kJ\ mol\ oxides^{-1}$ for the quenched and annealed glasses respectively.

The dissolution enthalpy of the α-cubic form of Na_2MoO_4 was measured and found to be ΔH_α = $-75.56 \pm 0.72\ kJ\ mol^{-1}$. One difficulty arises then from the fact that several allotropic forms of the mono-molybdate are detected in the samples. The transition enthalpies between the various allotropic forms are reported in table 4. The values from the CALPHAD assessment of

Bordier (44) are in good agreement with the compilation of Barin (49). In the balance calculations, Bordier values were adopted to maintain consistency in the comparison between experimental and modeling results. We have assumed that, as shown by the results of Nicoleau for quenched glasses having a MoO_3 content lower than 3 mol.%, the predominant form was the γ-orthorhombic one. Hence, we calculate: $\Delta H_{moly} = -98.85 \pm 0.72\ kJ\ mol^{-1} = -49.43 \pm 0.36\ kJ\ (mol\ oxide)^{-1}$.

We also assume that orthorhombic crystals are predominant in annealed glasses because of the slow cooling after the end of annealing that allows the transformation of the δ-hexagonal phase into the γ-orthorhombic phase.

The data reported in Figure 9 show that both methods, material balance and enthalpy balance give similar results.

3.4. CALPHAD calculations in the SiO_2-Na_2O-MoO_3 ternary

The metastable SiO_2-Na_2O-MoO_3 isothermal section at the synthesis temperature of the studied glasses 1300°C (1573K) is shown in Figure 10a. For the ternary composition $(80.4SiO_2\text{-}19.6Na_2O)_{1-x}(MoO_3)_x$ having a ratio $SiO_2/Na_2O \approx 4$ and representative of the quaternary experimental glasses $(63.5SiO_2\text{-}16.9B_2O_3\text{-}19.6Na_2O)_{1-x}(MoO_3)_x$ the MoO_3 increase above 3 mol.% leads to a separation between a molybdate rich liquid, close to the composition Na_2MoO_4, and a second silicate liquid, depleted in MoO_3 with a ratio $SiO_2/Na_2O \approx 4$.

At 990°C (1263 K, Fig. 10b), the metastable isothermal section is very similar to that at 1300°C, with the exception of the two-phase domain around Na_2O.

The isothermal metastable section calculated at 650°C (923 K, Fig. 10c) shows that the molybdate rich liquid is solidified as crystalline Na_2MoO_4. The liquid-liquid miscibility gap has changed to a two-phase liquid + solid Na_2MoO_4 domain which occupies the central part of the section.

The solidification path of a MoO_3-Na_2O-SiO_2 ternary glass having a ratio $SiO_2/Na_2O \approx 4$ and containing 3 mol.% MoO_3 is calculated in Figure 11. It is seen that, at 1600 K, two liquids already coexist. As the temperature is lowered, the quantity of silicate liquid gradually decreases with a corresponding increase in the quantity of molybdate liquid. This second liquid then solidifies at 953 K as crystalline Na_2MoO_4.

The evolution of the liquid-liquid phase separation temperature as a function of the MoO_3 content is compared for three distinct cases in Fig. 12: a binary liquid $(SiO_2)_{1-x}(MoO_3)_x$ (black solid line), a ternary one $(80SiO_2\text{-}20Na_2O)_{1-x}(MoO_3)_x$ (red solid line) and the quaternary experimental compositions $(64SiO_2\text{-}19Na_2O\text{-}17B_2O_3)_{1-x}(MoO_3)_x$. It can be seen that the

calculation overestimates the temperature of the phase separation most probably because B_2O_3 is only taken into account by an artificial increase in the silica content of the glass. Despite this obvious simplification, the shape of the calculated curve is very similar to the experimental one.

Calculations of precipitated phase fractions were also performed at 990°C, for compositions with MoO_3 content exceeding the solubility limit of quenched glasses, and at 650°C, for compositions with MoO_3 content exceeding the solubility limit of annealed glasses. These calculated precipitated fractions are compared to the fractions determined from the calorimetric experiments in Fig. 9.

4 Discussion

4.1. Solubility limit of molybdenum oxide

The experimental results obtained allow us to accurately determine the solubility limit of MoO_3 in two series of quenched and annealed quaternary glasses $(63.5SiO_2\text{-}19.6Na_2O\text{-}16.9B_2O_3)_{1-x}(MoO_3)_x$ with $0 \leq x \leq 3$ mol.% MoO_3.

The information given by HRTEM and acid solution enthalpy measurements agree to show the existence of separate phases in the quenched glasses from 1.5 mol.% MoO_3. This limit is detected by a slope break of the dissolution enthalpy as a function of the MoO_3 concentration and by the observation of spherical inclusions of nanometric sizes (Figure 3) dispersed in a homogeneous glass matrix. As indicated by HRTEM images, these inclusions are partially crystallized in glasses containing 1.5 mol.% MoO_3 and the presence of Na_2MoO_4 crystals is detected by PXRD from 1.8 mol.% MoO_3.

This result is in good agreement with the observations of Nicoleau et al. (24) on a series of similar glasses cooled under the same conditions. In this study, phase separation with partial crystallization into Na_2MoO_4 had been observed at the nanometer scale from 2 mol.% MoO_3. On increasing MoO_3 contents beyond 2% up to 10%, phase separation was observed at the microscopic (1 to 100 µm) and then macroscopic (> 100 µm) scales.

Compared to this previous study, the present work not only brings new experimental results in terms of solubility limit on both quenched and annealed glasses, but, by new in situ observations, allows to specify the temperature range in which the phase separation occurs. The value of the solubility limit (0.5 mol.% MoO_3) measured on the glasses annealed 10 h at 650°C is much lower than that measured on the quenched glasses (1.5 mol.% MoO_3). This can be explained considering that a fraction of the sodium and molybdenum amounts that remain dissolved, in a kind of supersaturated state, in the vitreous matrix of the quenched glasses, separates and forms sodium molybdates when the samples undergo an extended

stay in the metastable liquid state at 650°C, 140°C above the glass transition temperature, which is about 510°C in this type of glass.

Viscometry and ESEM in situ measurements in temperature allow to trace the evolution of the phase separation temperature up to a content of 3 mol.% of MoO_3. The molybdenum oxide content of the Na-M1.5 composition (1.5 mol.% MoO_3) coincides with the solubility limit of quenched glasses. For this glass, the phase separation temperature T_s is equal to 990°C (1263 K). We can then estimate that it is the state of the glass at 990°C which is observed after quenching at room temperature for this composition. All the quenched glasses having been cooled under the same conditions, we will consider that they all have been frozen at a temperature close to 990°C. This value can be used as a reference temperature for the comparison between the calculations and the precipitated fractions determined experimentally on the quenched glasses.

We have made the further assumption that the annealed glasses have reached a metastable equilibrium state after 10 h at 650°C (923 K). With this assumption, it can be considered that the solubility limit of the annealed glasses (0.5 mol.% MoO_3) has a separation temperature of 650°C. It can be verified in Fig. 12 that this experimental point extends the consistent trend drawn by the other points from the viscometry and ESEM measurements, thus validating somewhat the above hypothesis. Fig. 12 also shows that the overall shape of the extended experimental curve for quaternary compositions is very similar to that of the calculated curves for binary and ternary compositions. The annealing temperature can also be selected as a reference value for the comparison of calculated and experimental results on annealed glasses.

4.2. Nature and quantity of precipitates

Among sodium molybdates, the mono-molybdate (Na_2MoO_4) is the only secondary phase observed in Na-Mo*x* samples containing 0 to 3 mol.% MoO_3. It is also the one calculated at equilibrium with the Na_2O-SiO_2 melt using the CALPHAD model. For a more quantitative assessment, it is worth comparing the fractions of precipitates in the experiments and in the modelling. Fig. 9 shows that the experimental phase fractions are lower than the fractions calculated with the CALPHAD model for both quenched and annealed glasses but the magnitude of the discrepancy is somewhat larger for quenched glasses. A possible explanation could be that the rapid cooling of quenched samples limits the amount of precipitates that can nucleate and grow; thus, a fraction of molybdenum oxide is retained in the residual glass matrix of these samples. Whereas, in annealed glass, the more prolonged duration above the glass transition temperature favors precipitation and the evolution of the

precipitate fraction toward its metastable "equilibrium" value: the first solid molybdate to form at high temperature is in equilibrium with the Na_2O-SiO_2 melt.

For Na-Mo*x* samples containing molybdenum contents from 3 to 10 mol.% MoO_3, the study of Nicoleau et al. (24) showed that the crystalline phases consisted of a mixture of mono- and di-molybdates, with di-molybdates representing 13 to 29 wt.% of the total crystals. Regarding the considered Na_2O-SiO_2 ratio of the present experiments, this mixed precipitation is not calculated by the model in its current state of development. The addition in the model of boron and its interaction with sodium appears to be a prerequisite for further analysis of this discrepancy between model and experiment at high MoO_3 contents.

4.3. Relevance of experimental and modelling results for more complex glasses

In a previous study (9), the viscosity of three AMo*x* glasses with a composition close to that of industrial UMo glasses and molybdenum oxide contents equal to 5.1, 5.6 and 6.5 mol.% MoO_3 was measured at high temperatures. The phase separation temperatures could thus be determined with a protocol similar to that adopted in the present study. The experimental points corresponding to these three glasses have been plotted in Fig. 12 for comparison.

These experimental points suggest that the phase separation temperature increases slightly above 1400 K at high molybdenum oxide contents while the calculated phase separation temperature increases more steeply for both the MoO_3-SiO_2 binary and Na_2O-MoO_3-SiO_2 ternary cases. The phase separation temperatures calculated in these binary and ternary cases have very high values, largely above 2000 K, at the high MoO_3 contents of the AMo*x* glasses. This is not surprising because, in addition to boron, important chemical elements like Ca and Nd, which act as charge compensators for the MoO_4^{2-} units in borosilicate glasses (22, 30, 31, 50) are not taken into account in the CALPHAD modeling. More realistic estimate of the phase separation temperature of AMo*x* complex glasses is provided by simply extrapolating the results obtained at low MoO_3 contents on Na-Mo*x* quaternary compositions.

The present combined modeling and experimental approach shows that the key phenomena that can affect the proper functioning of the vitrification process, namely liquid-liquid phase separation and the resulting crystal precipitations, occur above the glass transition temperature. This means that, as a first step, it is not necessary to include the glass transition itself in the modelling approach to obtain relevant results and that modelling efforts should rather focus on improving the thermodynamic description of supercooled liquid and crystalline phases. The priority should be to include more chemical elements in the modelling, starting with boron and then calcium, a molybdate-forming element, both of which are expected to have a significant effect on the solubility of molybdenum oxide.

5 Conclusion and future work

The present study sheds new light on the thermodynamics of phase separation in sodium borosilicate nuclear glasses containing molybdenum oxide. Thanks to the coupling of several experimental techniques, both at room temperature and in situ at high temperature, it was possible to specify the compositional and temperature solubility limits for two series of quaternary SiO_2-B_2O_3-Na_2O-MoO_3 glasses, quenched or annealed, and to determine the nature and amount of the precipitated phases for the compositions beyond the solubility limits.

Thermodynamic calculations with the Thermo-Calc software and a CALPHAD database of the SiO_2-Na_2O-MoO_3 ternary, allowed a better interpretation of the experimental results thanks to the calculation of the solidification path of the liquid, even if, in the current state of development of the database, the absence of boron, still restricts the relevance of the model predictions. The experimental results acquired in this work constitute a first brick for the validation of a future more complete thermodynamic model, quaternary in a first step. The experimental methodology deployed here could allow the acquisition of data on a larger number of glass compositions.

Within the framework of the development of the 3rd generation databases, the thermodynamic description of the liquid phase using a 2-state model has been adopted in the CALPHAD community. Initiated on metallic elements, this new description of the liquid has been very recently extended to some simple oxides such as CaO (51), GeO_2 (52) and SiO_2 (53). A methodology coupling the 2-state model and the relaxation kinetics (54) has been proposed to simulate the glass transition. The integration of these potentially useful recent developments is a longer term perspective but the priority remains, for the application of the thermodynamic calculation tool to the vitrification process, to extend the current description to a larger number of elements. A validated calculation tool should make it possible to calculate *a priori* the phase separation temperature from the composition of the glass, and to adjust the molybdenum content of the glass so that the phase separation temperature remains below the synthesis temperature of the nuclear glass.

Acknowledgements

The authors are grateful to the Commissariat à l'énergie atomique et aux énergies alternatives (CEA), ORANO and EDF for their financial support of this work, the French scientific society for Thermodynamic of Materials (AFTherMat) where fruitful discussions started and led to collaborations on the present project, Martiane Cabié (CP2M, Aix-Marseille University) for informative discussion on HRTEM images and Emmanuelle Brackx (CEA, DES, ISEC, Université Montpellier, Marcoule, France) for EPMA.

Figure 1. Na_2O-SiO_2 mixing enthalpy. The calorimetric measurements (scatter symbols) by Fan at 1450 K (55) shows a smooth curve with a minimum around x_{SiO_2} = 0.4 characteristic of a sub regular attractive behavior in the liquid phase. The enthalpy curve calculated at 1380 K (solid line) using the thermodynamic database of Zhang et al (45) is plotted for comparison. The slope break of the calculated curve at x_{SiO_2} = 0.4, is associated with the formation of the $Na_6Si_2O_7$ crystalline compound at this lower temperature. In the two-phase region, the enthalpy of the solid + liquid mechanical mixture has a linear evolution vs. composition.

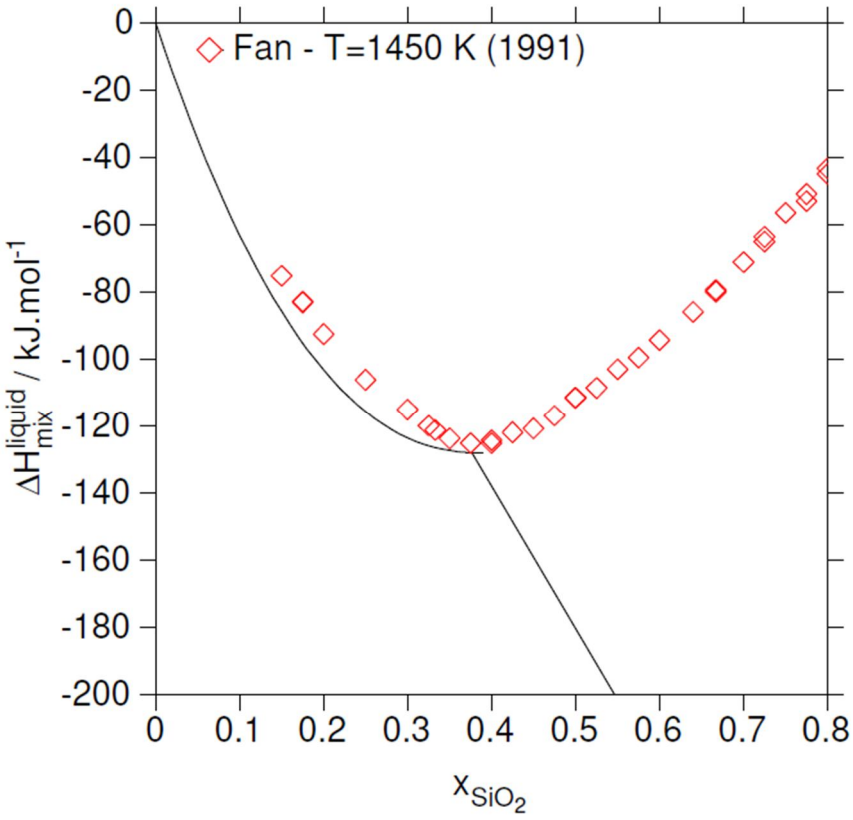

Figure 2. Visual inspection of the quenched and annealed Na-Mo*x* (*x* = 0 to 2.5 mol.%) glass series. Quenched glasses are visually transparent for MoO_3 < 2 mol.%. Above this concentration, the glasses are more and more opalescent and even milky white for the case of the Na-M2.5 glass. Annealed glasses are opalescent from and above 0.8 mol.% MoO_3.

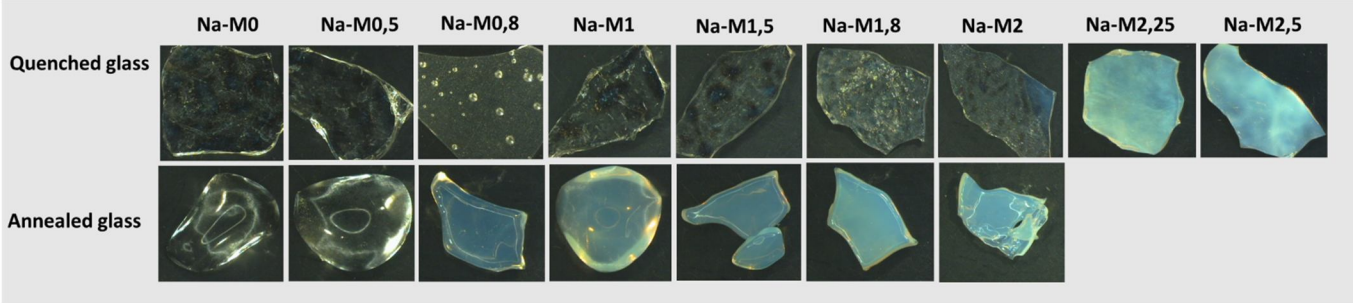

Figure 3. TEM images of the Na-Mo0 (a) and Na-Mo1.5 (b) quenched glasses. The dark area visible in the central part of Fig. 5a corresponds to a thickening of the glass grain that is homogeneous. Fig. 5b highlights the presence of predominantly globular inclusions in the glass matrix. A magnified HRTEM image of a nanometric precipitate is shown in the inlay of Fig. 5b. The inter-plane fringes show its crystalline character.

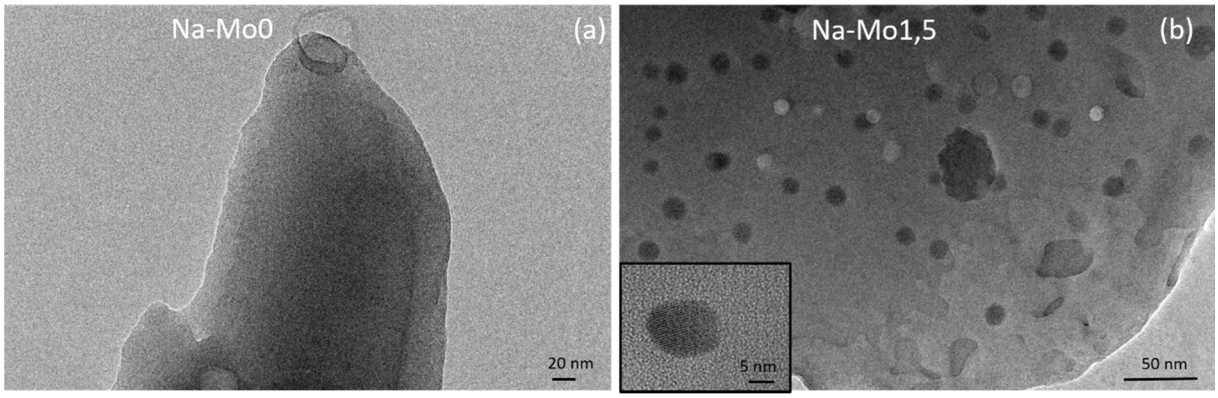

Figure 4: XRD patterns of the quenched (a) and annealed (b) Na-Mo*x* glasses.

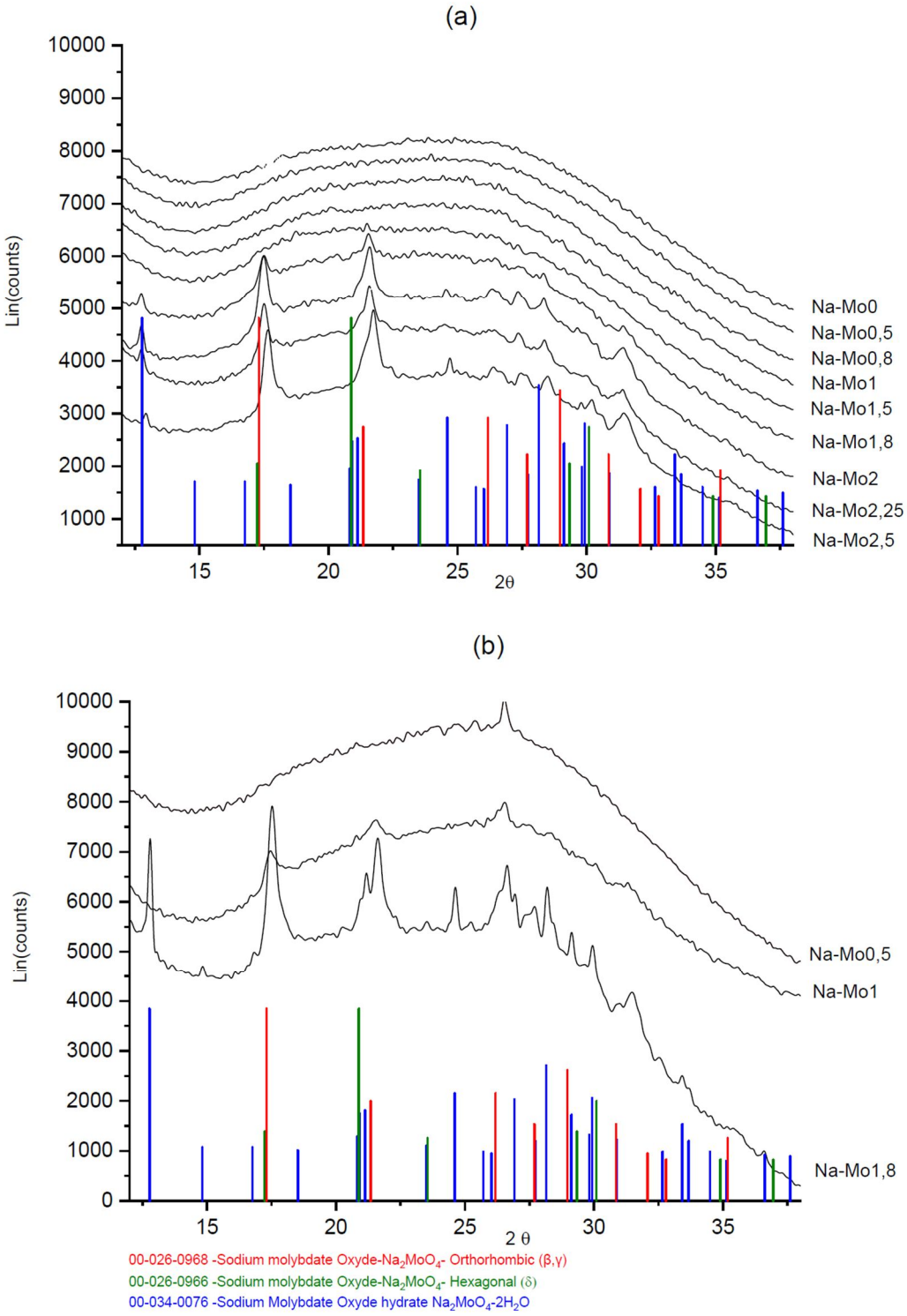

Figure 5: Viscosity of the Na-Mo*x* glasses.

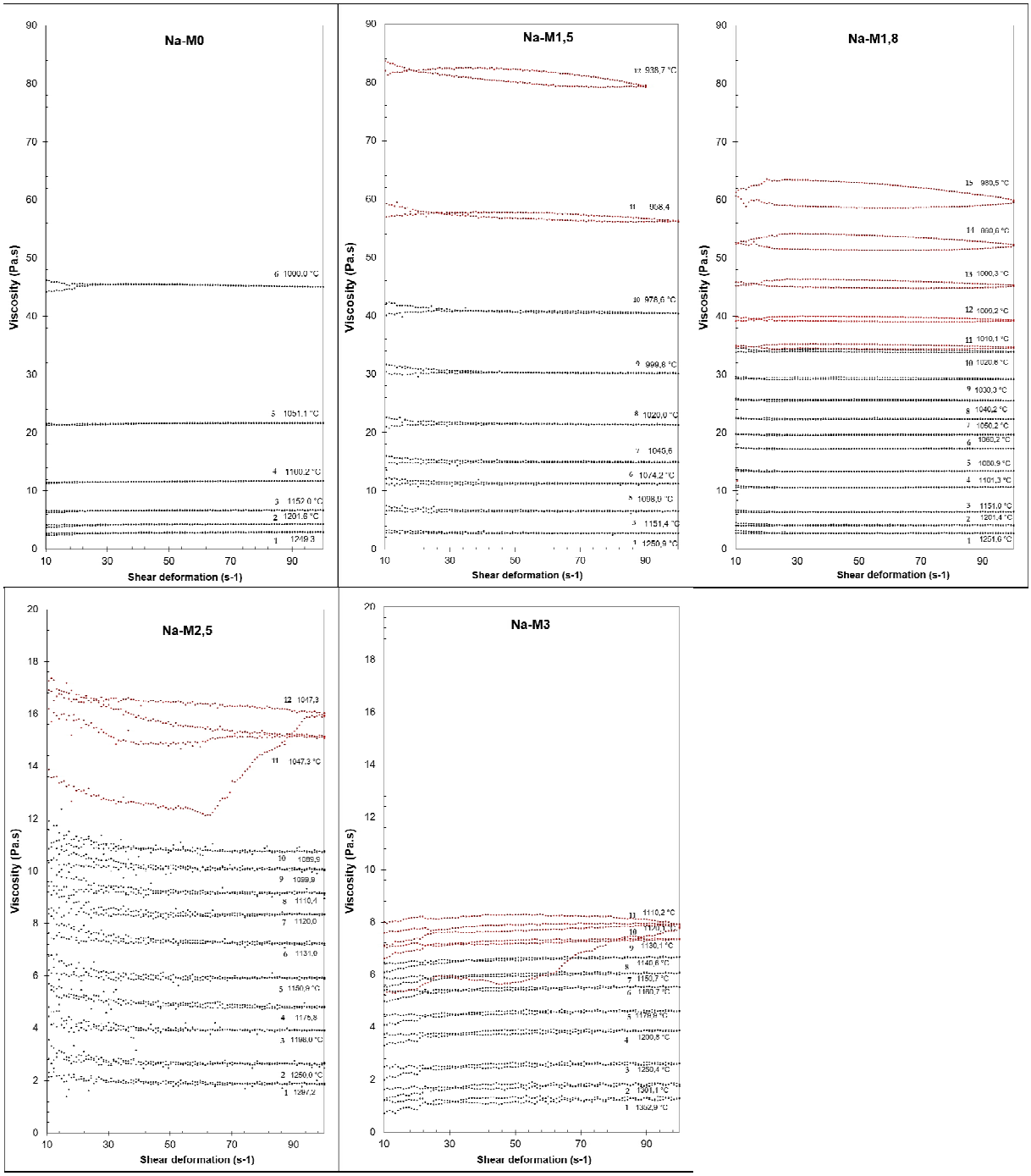

Figure 6: ESEM images of the Na-Mo1 quenched glass during heating from 652°C to 802°C. The liquid is fully homogeneous at 802°C. At 652°C and 745°C the upper images represent enlarged views of the zones identified by the black squares in the corresponding lower images. At 652°C and 702°C, the same precipitates are seen within the white squares.

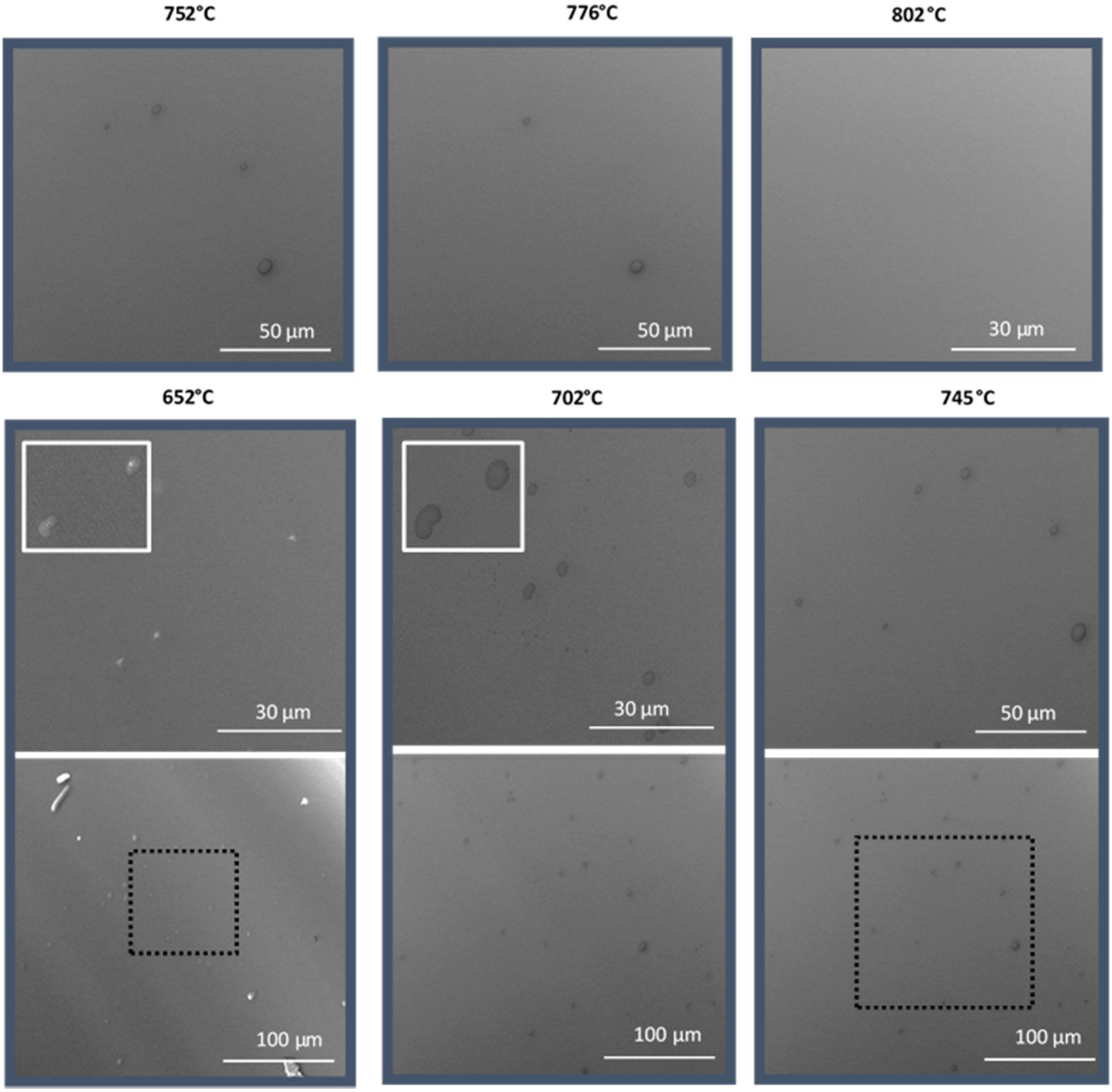

Figure 7: Evolution of the solution enthalpy of quenched Na-Mo*x* glasses as a function of MoO_3 content. (△) single-phase domain, (▲) two-phase domain. The dashed curve and the dotted line are only guides for the eye. The solubility limit is around 1.5 mol.% MoO_3.

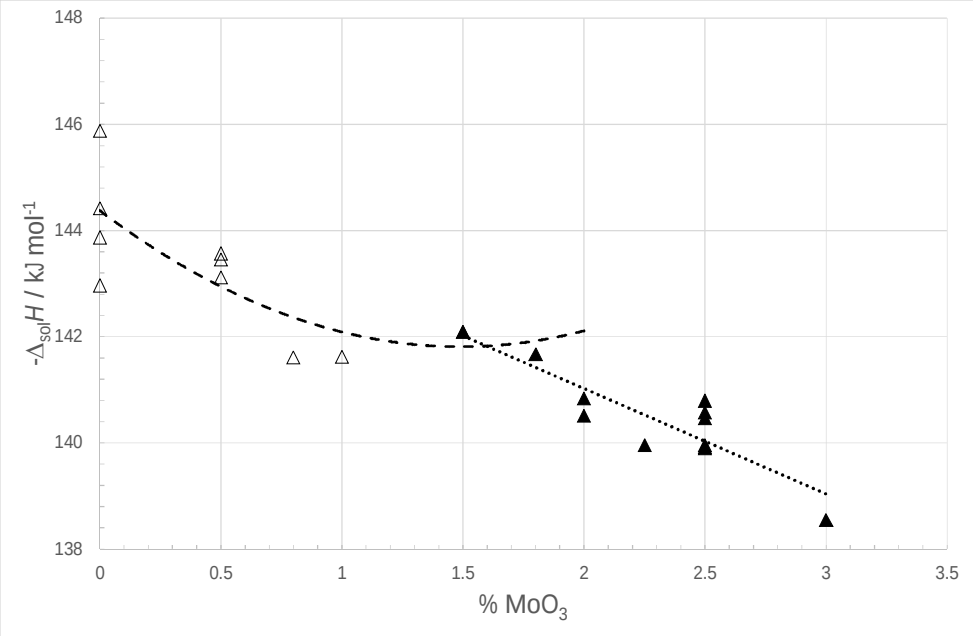

Figure 8: Evolution of the solution enthalpy of annealed Na-Mo*x* glasses as a function of MoO_3 content. (△) single-phase domain, (▲) two-phase domain. The dashed and dotted lines are only guides for the eye. The solubility limit is around 0.5 mol.% MoO_3.

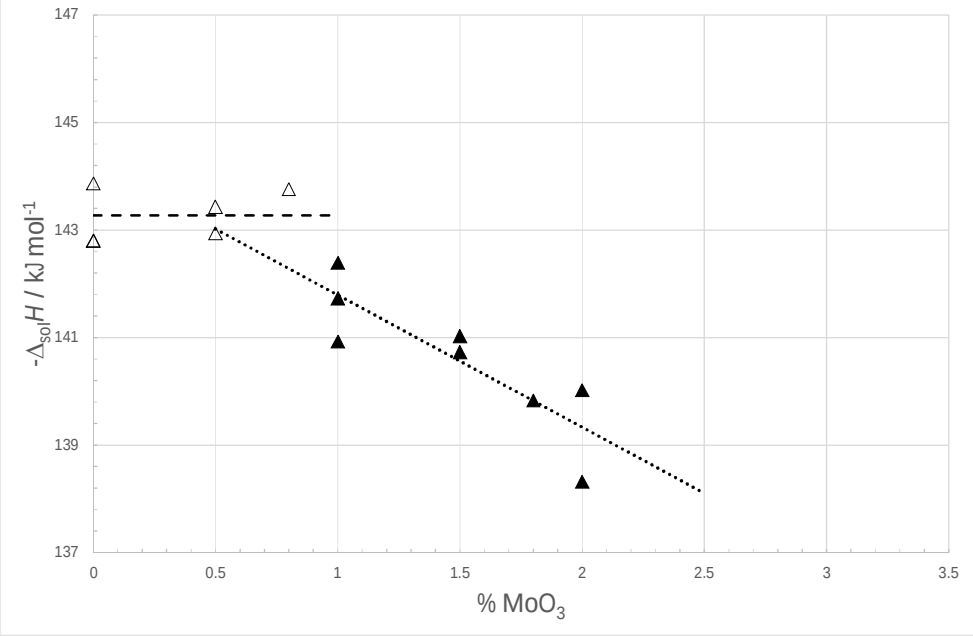

Figure 9. Precipitated fractions in Na-Mo*x* glasses determined from solution calorimetry experiments by MoO_3 material balance (○ symbols and dashed lines) and enthalpy balance (△ symbols) for both quenched (black) and annealed (red) glasses – Precipitated fractions calculated with Thermo-Calc and the ternary Na_2O-MoO_3-SiO_2 database from (44) are plotted as solid lines.

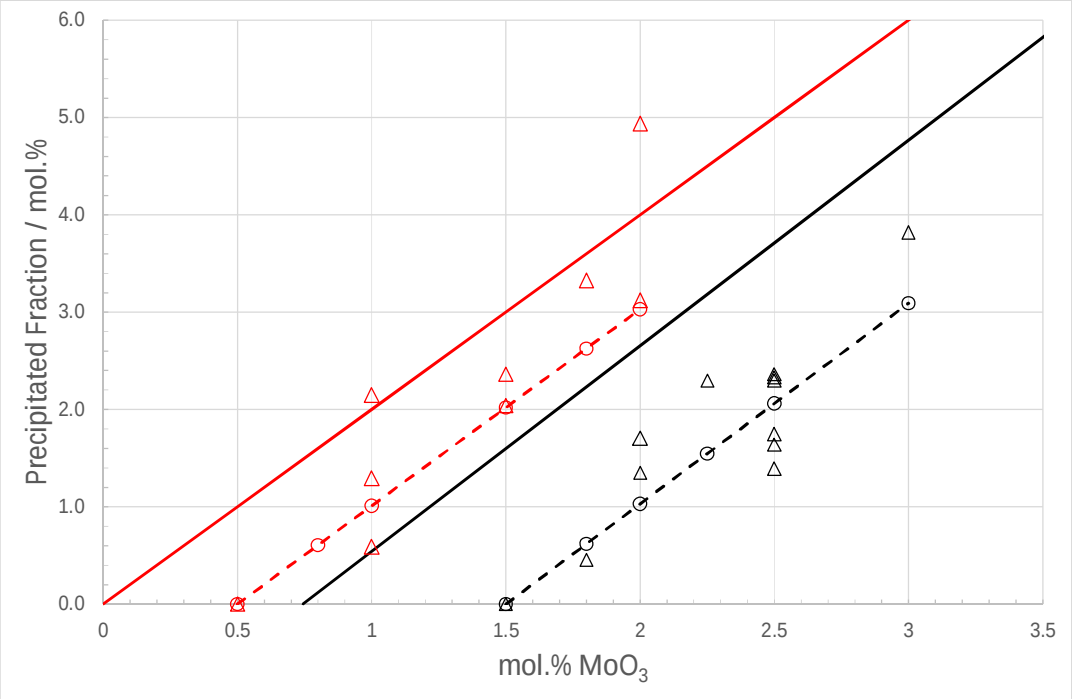

Figure 10. Metastable isothermal sections of the SiO_2-Na_2O-MoO_3 ternary diagram at a) 1300°C (1573 K), b) 990°C (1263 K) and c) 650°C (923 K). Solid straight lines are the tie-lines in the two phase domains.

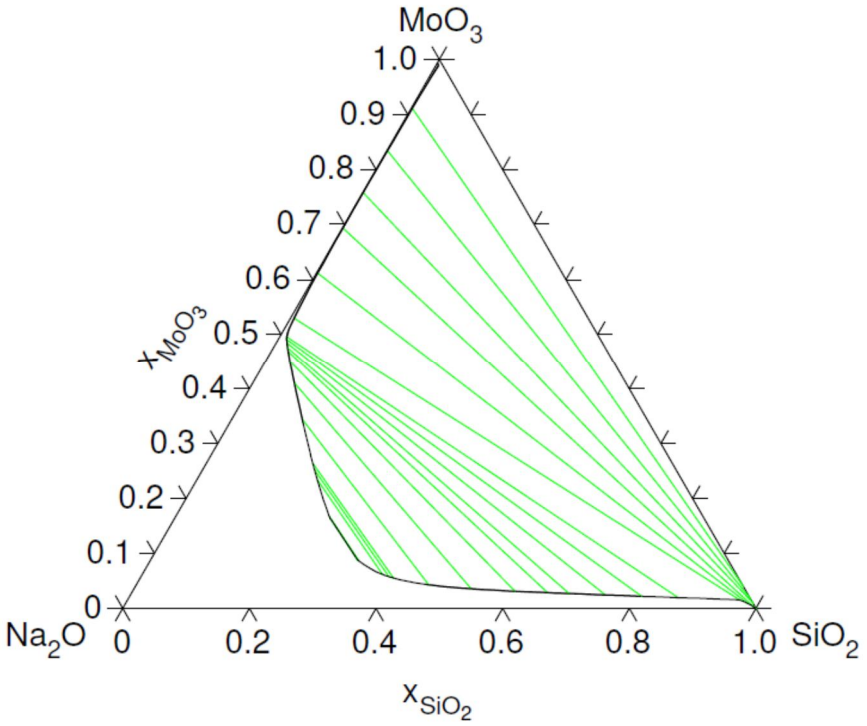

(a)

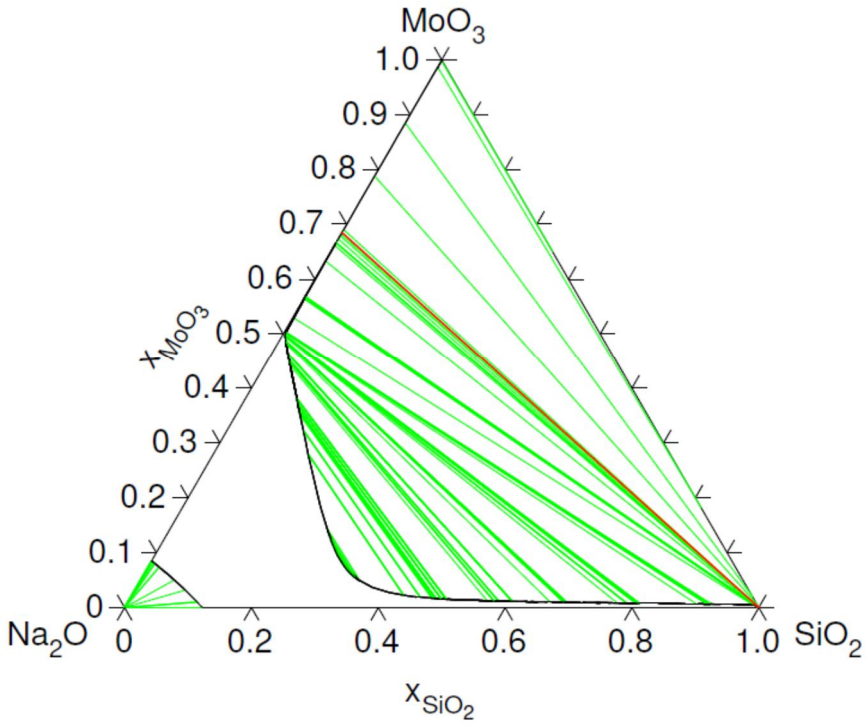

(b)

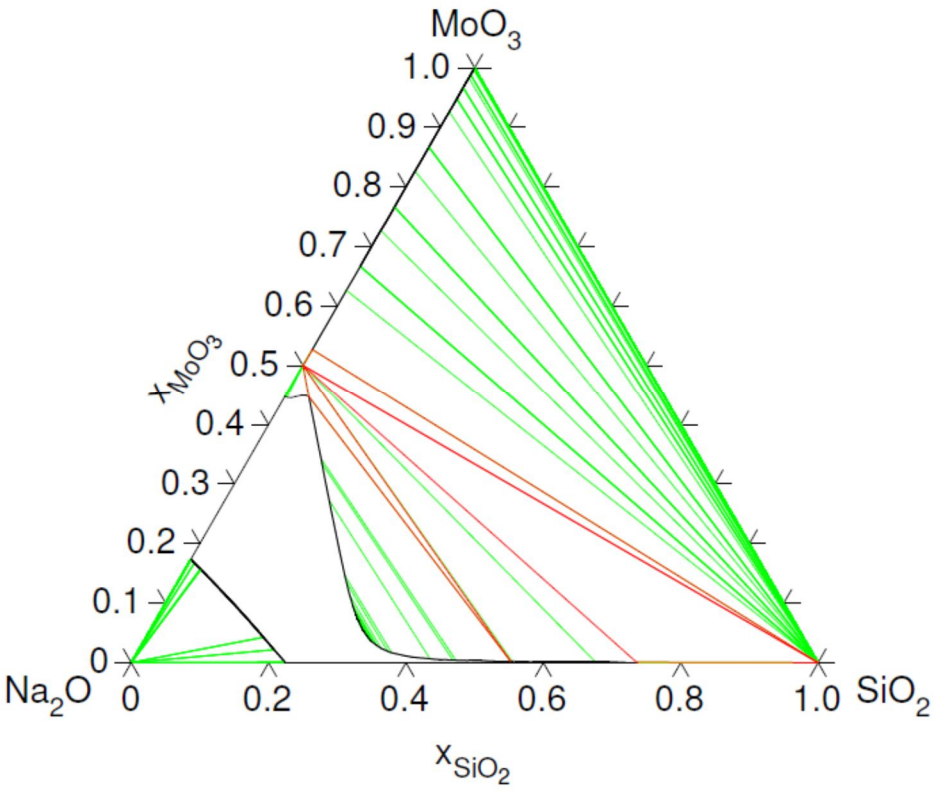

(c)

Figure 11. Calculated metastable solidification path of a MoO_3-Na_2O-SiO_2 ternary glass having a ratio $SiO_2/Na_2O \approx 4$ and containing 3 mol.% MoO_3.

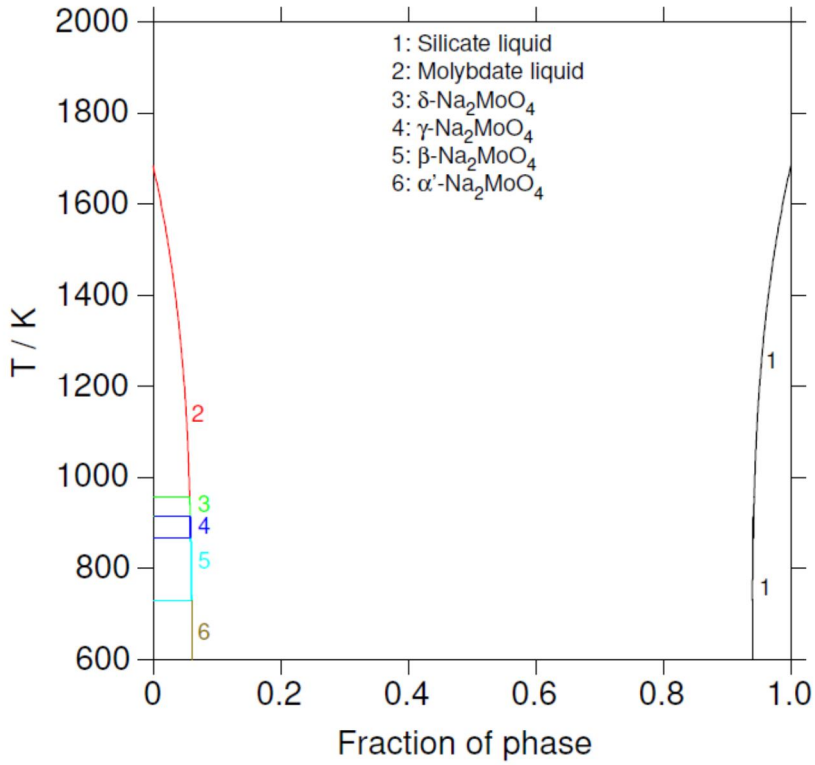

Figure 12: Phase separation temperatures calculated as a function of the MoO_3 content for SiO_2-MoO_3 binary (black solid line) and SiO_2-Na_2O-MoO_3 ternary (red solid line) compositions. Comparison with the phase separation temperatures measured in this work for the SiO_2-Na_2O-B_2O_3-MoO_3 quaternary glasses and in previous study on complex AMo*x* glass compositions (9).

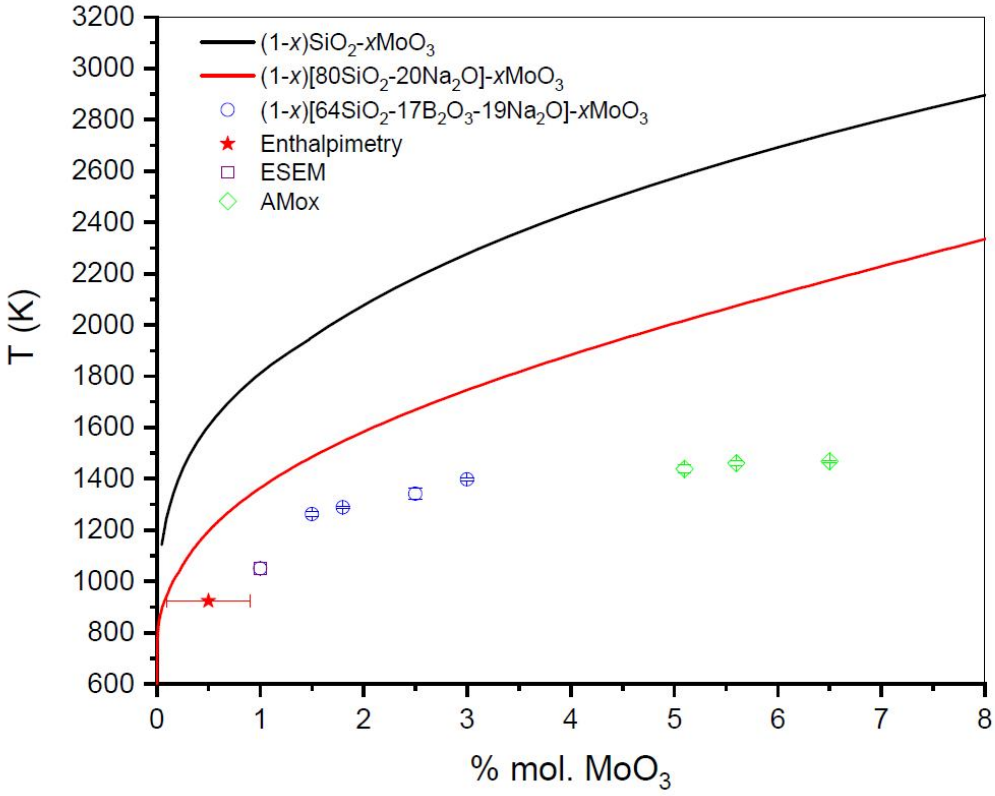

Tables

Table 1: Compositions of Na-Mo*x* glasses in mol.%. Theoretical compositions (%Th) calculated from weighing of the precursors and measured mass loss after the elaboration process and measured compositions (%An) determined by EPMA.

Mol.%	SiO_2 (%Th)	SiO_2 (%An)	σ%	B_2O_3 (%Th)	B_2O_3 (%An)	σ%	Na_2O (%Th)	Na_2O (%An)	σ%	MoO_3 (%Th)	MoO_3 (%An
Na-M0	63.49	63.95	0,5	16.91	16.34	0,3	19.60	19.71	0,5	0.00	0.00
Na-M0.5	63.18	64.39	0,7	16.82	16.35	0,5	19.50	18.76	0,5	0.50	0.51
Na-M0.8	62.99	-		16.77	-		19.44	-		0.80	-
Na-M1	62.86	62.74	0,2	16.74	15.96	0,4	19.40	20.28	0,1	1.00	1.03
Na-M1.5	62.54	63.19	0,3	16.65	15.65	0,2	19.31	19.67	0,5	1.50	1.49
Na-M1.8	62.35	-		16.60	-		19.25	-		1.80	-
Na-M2	62.22	62.22	0,3	16.57	16.16	0,2	19.21	19.56	0,1	2.00	2.07
Na-M2.25	62.07	-		16.53	-		19.16	-		2.25	-
Na-M2.5	61.91	-		16.48	-		19.11	-		2.50	-
Na-M3	61.59	-		16.40	-		19.01	-		3.00	-

Table 2: Phase separation temperatures of Na-Mo*x* glass series. For viscometry experiments, T_{min}s is the lowest temperature at which the liquid has a Newtonian behavior and T_{max}s is the highest temperature at which the liquid has a non-Newtonian behavior. For ESEM experiment, T_{max}s is the highest temperature at which the liquid is heterogeneous and T_{min}s is the lowest temperature at which the melt is homogeneous. T_s is the average of T_{min}s and T_{max}s values.

Glass	**T_{min}s (°C)**	**T_{max}s (°C)**	**T_s (°C)**	**Estimated standard deviation (°C)**	**Experimental technique**
Na-M1	802	752	777	25	ESEM
Na-Mo1.5	1000	979	989.5	10.5	Viscometry
Na-Mo1.8	1021	1009	1015	6	Viscometry
Na-Mo2.5	1090	1047	1068.5	21.5	Viscometry
Na-Mo3	1140	1130	1135	5	Viscometry

Table 3: Dissolution enthalpies ($\Delta_{sol}H$), fractions of precipitated phase in the quenched and annealed glasses, determined by mass (F_m) and enthalpy (F_h) balances from solution calorimetry results. All % are mol. %.

Quenched glasses				Annealed glasses			
MoO_3 / %	$\Delta_{sol}H$ / kJ mol oxide^{-1}	F_h / %	F_m / %	MoO_3 / %	$\Delta_{sol}H$ / kJ mol oxide^{-1}	F_h / %	F_m / %
0	-145.88			0	-143.87		
0	-142.97			0	-142.8		
0	-143.87			0	-142.81		
0	-144.42			0.5	-142.94	0.00	
0.5	-143.57			0.5	-143.43	-	0.00
0.5	-143.46			0.8	-143.76	-	
0.5	-143.12			1	-141.73	1.29	
0.8	-141.61			1	-140.93	2.15	0.61
1	-141.62			1	-142.39	0.59	1.01
1.5	-142.09	0.00	0.00	1.5	-141.03	2.04	2.02
1.8	-141.67	0.45	0.62	1.5	-140.73	2.36	2.63
2	-140.84	1.35	1.03	1.8	-139.83	3.33	3.03
2	-140.51	1.71		2	-140.02	3.12	
2.25	-139.96	2.30	1.55	2	-138.32	4.94	
2.5	-139.9	2.36	2.06				
2.5	-139.96	2.30					
2.5	-140.47	1.75					
2.5	-140.57	1.64					
2.5	-140.8	1.39					
2.5	-139.93	2.33					
3	-138.55	3.82	3.09				

Table 4. Transition temperatures (T_{trs}) and enthalpies $\Delta_{\mathrm{trs}}H$ between the allotropic α (cubic), β (unknown structure), γ (orthorhombic) and δ (hexagonal) forms of Na_2MoO_4 according to Barin (49) and Bordier (44).

Reference	Barin		Bordier	
Transition	T_{trs} / °C	$\Delta_{\mathrm{trs}}H$ / kJ mol^{-1}	T_{trs} / °C	$\Delta_{\mathrm{trs}}H$ / kJ mol^{-1}
$\alpha' \leftrightarrow \beta$	451	23.430	457	20.623
$\beta \leftrightarrow \gamma$	585	2.008	593	2.674
$\gamma \leftrightarrow \delta$	635	9.121	640	8.733
$\delta \leftrightarrow$ L	688	22.426	684	20.640

References

1. Suzuki M, Tanaka T. Thermodynamic Prediction of Spinodal Decomposition in Multi-component Silicate Glass for Design of Functional Porous Glass Materials %J High Temperature Materials and Processes. 2012;31(4-5):323-8.
2. Kim SS, Sanders TH. Phase-field simulation of spinodal phase separation in the Na2O-SiO2 glasses. Journal of Non-Crystalline Solids. 2020;528:119591.
3. Varshneya AK, Mauro JC. Chapter 4 - Glass microstructure: Phase separation and liquid immiscibility. In: Varshneya AK, Mauro JC, editors. Fundamentals of Inorganic Glasses (Third Edition): Elsevier; 2019. p. 71-100.
4. Zanotto ED. Effect of liquid phase separation on crystal nucleation in glass-formers. Case closed. Ceramics International. 2020;46(16, Part A):24779-91.
5. Ertuş EB, Vakifahmetoglu C, Öztürk A. Production and properties of phase separated porous glass. Ceramics International. 2020;46(4):4947-51.
6. Huang X. Manufacture of porous glass. Journal of Non-Crystalline Solids. 1989;112(1):58-63.
7. Pinet O, Dussossoy JL, David C, Fillet C. Glass matrices for immobilizing nuclear waste containing molybdenum and phosphorus. Journal of Nuclear Materials. 2008;377(2):307-12.
8. Pinet O, Hollebecque JF, Hugon I, Debono V, Campayo L, Vallat C, et al. Glass ceramic for the vitrification of high level waste with a high molybdenum content. Journal of Nuclear Materials. 2019;519:121-7.
9. Schuller S, Pinet O, Penelon B. Liquid–Liquid Phase Separation Process in Borosilicate Liquids Enriched in Molybdenum and Phosphorus Oxides. 2011;94(2):447-54.
10. McCloy JS, Riley BJ, Crum J, Marcial J, Reiser JT, Kruska K, et al. Crystallization study of rare earth and molybdenum containing nuclear waste glass ceramics. 2019;102(9):5149-63.
11. Crum JV, Turo L, Riley B, Tang M, Kossoy A. Multi-Phase Glass-Ceramics as a Waste Form for Combined Fission Products: Alkalis, Alkaline Earths, Lanthanides, and Transition Metals. Journal of the American Ceramic Society. 2012;95(4):1297-303.
12. Crum J, Maio V, McCloy J, Scott C, Riley B, Benefiel B, et al. Cold crucible induction melter studies for making glass ceramic waste forms: A feasibility assessment. Journal of Nuclear Materials. 2014;444(1):481-92.
13. Achigar S, Caurant D, Régnier E, Majérus O. Dismantling nuclear waste rich in P2O5, MoO3 and ZrO2: How do these oxides incorporate in aluminoborosilicate glasses? Journal of Nuclear Materials. 2021;544:152731.
14. Allix M, Cormier L. Crystallization and Glass-Ceramics. In: Musgraves JD, Hu J, Calvez L, editors. Springer Handbook of Glass. Cham: Springer International Publishing; 2019. p. 113-67.
15. McCloy JS, Schuller S. Vitrification of wastes: from unwanted to controlled crystallization, a review. Comptes Rendus Géoscience 2022:pp. 1-40. .
16. Caurant D, Majérus O. Glasses and Glass-Ceramics for Nuclear Waste Immobilization. Reference Module in Materials Science and Materials Engineering: Elsevier; 2021.
17. Pinet O, Grandjean A, Frugier P, Rabiller H, Poissonnet S. Leaching behavior of a polyphase glass–ceramic containment matrix. Journal of Non-Crystalline Solids. 2006;352(28):3095-102.
18. Uruga K, Tsukada T, Usami T. Generation mechanism and prevention method of secondary molybdate phase during vitrification of PUREX wastes in liquid-fed ceramic melter. Journal of Nuclear Science and Technology. 2020;57(4):433-43.
19. Short RJ, Hand RJ, Hyatt NC. Molybdenum in Nuclear Waste Glasses - Incorporation and Redox state. MRS Proceedings. 2002;757:II5.4.
20. Farges Fo, Siewert R, Brown GE, Jr., Guesdon A, Morin G. STRUCTURAL ENVIRONMENTS AROUND MOLYBDENUM IN SILICATE GLASSES AND MELTS. I. INFLUENCE OF COMPOSITION AND OXYGEN FUGACITY ON THE LOCAL STRUCTURE OF MOLYBDENUM. The Canadian Mineralogist. 2006;44(3):731-53.
21. Calas G, Le Grand M, Galoisy L, Ghaleb D. Structural role of molybdenum in nuclear glasses: an EXAFS study. Journal of Nuclear Materials. 2003;322(1):15-20.

22. Caurant D, Majérus O, Fadel E, Quintas A, Gervais C, Charpentier T, et al. Structural investigations of borosilicate glasses containing MoO3 by MAS NMR and Raman spectroscopies. Journal of Nuclear Materials. 2010;396(1):94-101.
23. Magnin M., Schuller S., Caurant D.,Majérus O., de Ligny D. Phase separation and crystallization in soda-lime borosilicate glass enriched in MoO3 studied by in situ Raman spectroscopy at high temperature. ⟨hal-00994577⟩2008.
24. Nicoleau E, Schuller S, Angeli F, Charpentier T, Jollivet P, Le Gac A, et al. Phase separation and crystallization effects on the structure and durability of molybdenum borosilicate glass. Journal of Non-Crystalline Solids. 2015;427:120-33.
25. Boué E, Schuller S, Toplis MJ, Charpentier T, Mesbah A, Pablo H, et al. Kinetic and thermodynamic factors controlling the dissolution of molybdate-bearing calcines during nuclear glass synthesis. Journal of Nuclear Materials. 2019;519:74-87.
26. Martineau C, Michaelis VK, Schuller S, Kroeker S. Liquid–Liquid Phase Separation in Model Nuclear Waste Glasses: A Solid-State Double-Resonance NMR Study. Chemistry of Materials. 2010;22(17):4896-903.
27. Magnin M, Schuller S, Mercier C, Trébosc J, Caurant D, Majérus O, et al. Modification of molybdenum structural environment in borosilicate glasses with increasing content of boron and calcium oxide by 95Mo MAS NMR. Journal of the American Ceramic Society. 2011;94(12):4274-82.
28. Schuller S, Pinet O, Grandjean A, Blisson T. Phase separation and crystallization of borosilicate glass enriched in MoO3, P2O5, ZrO2, CaO. Journal of Non-Crystalline Solids. 2008;354(2):296-300.
29. Kroeker S, Schuller S, Wren JEC, Greer BJ, Mesbah A. 133Cs and 23Na MAS NMR Spectroscopy of Molybdate Crystallization in Model Nuclear Glasses. Journal of the American Ceramic Society. 2016;99(5):1557-64.
30. Chouard N, Caurant D, Majérus O, Guezi-Hasni N, Dussossoy J-L, Baddour-Hadjean R, et al. Thermal stability of SiO2–B2O3–Al2O3–Na2O–CaO glasses with high Nd2O3 and MoO3 concentrations. Journal of Alloys and Compounds. 2016;671:84-99.
31. Patil DS, Konale M, Gabel M, Neill OK, Crum JV, Goel A, et al. Impact of rare earth ion size on the phase evolution of MoO3-containing aluminoborosilicate glass-ceramics. Journal of Nuclear Materials. 2018;510:539-50.
32. Patel KB, Schuller S, Lampronti GI, Farnan I. Mechanism of powellite crystallite expansion within nano-phase separated amorphous matrices under Au-irradiation. Physical chemistry chemical physics : PCCP. 2020;22(27):15616-31.
33. Benigni P, Rogez J, Schuller S. Experimental Determination of Thermodynamical Quantities in Oxide Mixtures and Glasses. Procedia Materials Science. 2014;7:138-47.
34. Gossé S, Guéneau C, Bordier S, Schuller S, Laplace A, Rogez J. A Thermodynamic Approach to Predict the Metallic and Oxide Phases Precipitations in Nuclear Waste Glass Melts. Procedia Materials Science. 2014;7:79-86.
35. Prosen EJ, Kilday MV. Enthalpies of Reaction of Tris(hydroxymethyl)aminomethane in HCl(aq) and in NaOH(aq). J Res Natl Bur Stand A Phys Chem. 1973;77A(5):581-97.
36. Takamori T, Tomozawa M. Viscosity and Microstructure of Phase-Separated Borosilicate Glasses. Journal of the American Ceramic Society. 1979;62(7-8):373-7.
37. Tomozawa M, Sridharan S, Takamori T. Origin of Viscosity Increase of Phase-Separated Borosilicate Glasses. Journal of the American Ceramic Society. 1992;75(11):3103-10.
38. Mazurin OV, Roskova GP, Kluyev VP. Properties of phase-separated soda-silica glasses as a means of investigation of their structure. Discussions of the Faraday Society. 1970;50(0):191-9.
39. Deubener J. Viscosity of Glass-Forming Melts. Encyclopedia of Glass Science, Technology, History, and Culture 2021. p. 431-51.
40. Podor R, Schuller S, Ravaux J, Monteiro A, Boucetta H, Delattre O, et al. In Situ ESEM Experiment Applied to the Description of Chemical Processes during Glass Elaboration. Procedia Materials Science. 2014;7:111-6.
41. Podor R, inventorSample holder with integrated thermocouple 2013.

42. Lukas H, Fries SG, Sundman B. Computational Thermodynamics: The Calphad Method. Cambridge: Cambridge University Press; 2007.
43. Andersson J-O, Helander T, Höglund L, Shi P, Sundman BJC-cCoPD, Thermochemistry. Thermo-Calc & DICTRA, computational tools for materials science. 2002;26:273-312.
44. Bordier S. Modélisation thermodynamique des phases insolubles dans les verres nucléaires : application à la vitrification du molybdène et des produits de fission platinoïdes 2015.
45. Zhang L, Schmetterer C, Masset PJ. Thermodynamic description of the M2O–SiO2 (M=K, Na) systems. Computational Materials Science. 2013;66:20-7.
46. Stemprok. M VJ. Homogenni Skla v systémech Na_2O-SiO_2-WO3 a Na_2O-SiO_2-MoO_3. Silikaty. 1974;1:19-30.
47. Stemprok. M S. Geological significance of immicibility in fused silicate systems containing tunsgten and molybdenum Industrial & Engineering Chemistry. 1975;17.
48. Singh Mudher KD, Keskar M, Krishnan K, Venugopal V. Thermal and X-ray diffraction studies on Na2MoO4, Na2Mo2O7 and Na2Mo4O13. Journal of Alloys and Compounds. 2005;396(1):275-9.
49. Barin. Thermochemical Data of Pure Substances (3rd ed.). Weinheim; New York; Basel; Cambridge; Tokyo: VCH.1995.
50. Magnin M. Etude des processus de démixtion et de cristallisation au sein de liquides fondus borosilicatés riches en oxyde de molybdène 2009.
51. Deffrennes G, Jakse N, Alvares CMS, Nuta I, Pasturel A, Khvan A, et al. Thermodynamic modelling of the Ca–O system including 3rd generation description of CaO and CaO2. Calphad. 2020;69:101764.
52. Bajenova I, Khvan A, Derevyanko M, Aristova N, Dinsdale A, Kondratiev A, et al. Third-generation CALPHAD description of pure GeO2 at 1 atm. Calphad. 2021;74:102299.
53. Bajenova I, Khvan A, Dinsdale A, Kondratiev A. Implementation of the extended Einstein and two-state liquid models for thermodynamic description of pure SiO2 at 1 atm. Calphad. 2020;68:101716.
54. Benigni P. CALPHAD modeling of the glass transition for a pure substance, coupling thermodynamics and relaxation kinetics. 2021;72:102238.
55. Fan M. Thermochemische Untersuchung Der Schmelzen Na_2O-SiO_2, Na_2O-GeO_2, Na_2O-B_2O_3 Und Li_2O-B_2O_3: RWTH, Aachen, Germany; 1991.
56. Barlow ST, Fisher AJ, Bailey DJ, Blackburn LR, Stennett MC, Hand RJ, et al. Thermal treatment of nuclear fuel-containing Magnox sludge radioactive waste. Journal of Nuclear Materials. 2021:152965.
.